COMMUNICATIONS IN SCIENCE AND TECHNOLOGY
Homepage: cst.kipmi.or.id

Utilization of glycerol solution for hydrogen production by a combination of photocatalysis and electrolysis processes with Fe-TiO_2 nanotubes

Calvin Santoso[a], Ratnawati[b], Slamet[a,*]

[a]*Department of Chemical Engineering, Faculty of Engineering, Universitas Indonesia, Depok 16424, Indonesia*
[b]*Department of Chemical Engineering, Institut Teknologi Indonesia, Serpong 15314, Indonesia*

Article history:
Received: 23 September 2023 / Received in revised form: 14 December 2023 / Accepted: 14 December 2023

Abstract

A combination of photocatalysis and electrolysis (photoelectrocatalysis) for the simultaneous degradation of glycerol and hydrogen production using Fe-TiO_2 nanotubes has been studied. This photocatalyst was synthesized through Ti anodization followed by Fe deposition with $Fe(NO_3)_3$ as precursor using the SILAR (successive ionic layer adsorption and reaction) method. The effects of Fe loading (based on the number of SILAR cycles) on TiO_2 nanotubes and glycerol concentration were examined. The generated TiO_2 nanotubes were 100% anatase phase with crystallite size between 25 and 29 nm. The results of UV-Vis DRS showed that the number of SILAR cycles of Fe dopant determined the magnitude of the decrease in the band gap of photocatalysts up to 2.74 eV, notably lower than a typical value of 3.15 eV associated with TiO_2 anatase. FESEM/EDX, TEM, and HRTEM characterizations indicated the formation of neatly arranged TiO_2 nanotubes with Fe deposited on the surface. The photoelectrocatalytic process increased the hydrogen produced by up to 5 times compared to a single photocatalytic or electrolysis process. The photocatalyst sample with Fe deposited on TiO_2 nanotubes via a SILAR method with 15 cycles outperformed its bare TiO_2 nanotube counterpart by producing hydrogen by 2.5 times (405.8 mmol/m^2). Glycerol photo-reforming at 10% concentration produced hydrogen 6 times greater than water splitting (0% glycerol).

Keywords: Photoelectrocatalysis, Fe-TiO_2 Nanotubes, Glycerol, Hydrogen

1. Introduction

Glycerol solution, a biomass-derived waste, is a by-product of the biodiesel industry that has not been optimally used. The abundant availability due to the limited demand in the market has decreased the selling value. It cannot be directly discharged into the environment in view of the high organic matter content and tendency to damage the environment [1,2]. Furthermore, 100 kg of glycerol can be obtained in every ton of biodiesel converted from biomass [1] where biodiesel is an alternative green fuel [3]. Also, glycerol presents a particularly attractive renewable and sustainable source for H_2 generation. Therefore, a treatment process such as photocatalysis needs to be carried out to effectively utilize the waste, such as glycerol, since it is a promising method to oxidize any harmful organic and inorganic pollutants [4]. Glycerol can be used as a renewable resource in H_2 production. Hydrogen, a renewable and clean energy, must be concerned due to the depletion of fossil fuels, environmental issues, and increasing global energy demand. Thus, the generation of H_2 and pollutant removal is expected to occur simultaneously [5].

Photocatalysis is a photochemical reaction involving light and a catalyst material to speed up a chemical reaction. To obtain an effective photocatalyst, several parameters need to be considered, including morphology/size, surface chemistry of catalyst, type of material, crystal structure and size, addition of dopants and conditions of the photocatalysis process [6-8]. Light exposure to a semiconductor catalyst excites electrons from the valence to the conduction band to form the pairs of electrons (e-) and holes (h^+), separated into free photoelectrons in the conduction band and photo holes in the valence band. The hole reacts with water to form hydroxyl radicals, which reduce organic compounds into CO_2 and H_2O [9]. The hydroxyl radicals generated are highly reactive and can mineralize organic compounds [10]. The electrons reduce the hydrogen ions to hydrogen gas (H_2). However, photocatalysis has several weaknesses, including the rapid recombination of electrons and holes generated from the photocatalytic process.

To prevent the recombination of electrons and holes, a combination of photocatalysis and electrolysis (photo electrocatalytic processes/PEC) can be carried out using an externally applied electric bias [1]. At this point, the electrolysis process can directly transfer the electrons, which are generated from the photocatalysis process to reduce H^+ to H_2, a renewable energy replacing fossil fuels. The combination of photocatalytic and electrolysis processes is also expected to increase the amount of hydrogen produced. Additionally, to reduce the electron-hole recombination process, a sacrificial agent such as glycerol is required [5]. A sacrificial agent is a

* Corresponding author.
Email: slamet@che.ui.ac.id
https://doi.org/10.21924/cst.8.2.2023.1280

hole scavenger/electron donor, capable of decreasing the tendency of electron and hole recombination and accelerating the hydrogen generation rate [11]. Glycerol is an excellent hole scavenger and is easy to oxidize. Splitting of water and photo-reforming of glycerol are believed to take place simultaneously in the absence of oxygen. Hydrogen production is significantly improved as the glycerol is oxidized by holes, OH radicals, and oxygen produced by water cleavage. Furthermore, introducing glycerol into the photocatalytic system also suppresses O_2-H_2 back reaction [12].

Besides reducing recombination, glycerol as a sacrificial agent can also function as a reactant in producing hydrogen. This is because glycerol contains H atoms whose oxidation results produce H_2, thereby kinetically increasing the formation of hydrogen. In this case, glycerol waste (pollutant) can be chemically converted into renewable energy such as H_2 [14]. Many researchers have studied the optimal initial glycerol concentration for the photocatalytic process. Unfortunately, studies about the effect of the initial concentration of glycerol on the photoelectrocatalytic process, so far, are rarely performed. Therefore, further investigation needs to be carried out. Previous studies included glycerol oxidation using the PEC process with WO_3, WO_3/TiO_2, W-$BiVO_4$ and other photocatalysts [1,2].

The most popular semiconductor material photocatalyst is TiO_2 due to its high photocatalytic activity, nontoxicity, cost-effectiveness/affordability, corrosion resistance, and environmental friendliness [15,16]. Along with these advantages, there are some drawbacks, however. Besides having a higher recombination rate of photogenerated electrons (e^-) and holes (h^+), TiO_2 also has a relatively wide band gap and low surface area [15,17]. The recombination should be eliminated since it prevents the occurrence of the oxidation-reduction reaction on the photocatalyst's surface, which reduces its effectiveness in its application. Meanwhile, with the wide band gap (3-3.2 eV), TiO_2 can only be activated by exposure to ultraviolet light. To enhance the efficiency in its applications, TiO_2 is modified into TiO_2 nanotube arrays (TiNTAs) with a neatly arranged and vertical tube morphology. Of the various forms of nanotubes available, semiconductor TiNTAs are demanded at most [18] since they absorb photons more efficiently without overlapping TiO_2 nanotubes. Therefore, photon absorption with TiNTAs morphology is considered better.

Various metallic or non-metallic dopants have been used to enhance TiO_2 photocatalytic activity, such as N, B, C, Cl, Fe, Mo, V, Co, and Cu [6, 14, and 19]. Compared to other elements, TiO_2 modified with iron (Fe) dopants strongly supports photocatalytic performance because Fe^{3+} easily fits into the TiO_2 lattice due to its ionic radius (0.64 Å), similar to Ti^{4+} (0.68 Å). Iron is one of Earth's most abundant, affordable, and non-toxic elements. TiO_2 nanotube photocatalyst modified with Fe dopant is used as an electron and hole trapper, which can reduce the electron-holes recombination rate and narrow the band gap [20], effectively enhancing the photoelectrocatalytic process.

The amount of Fe dopant deposited on TiO_2 determines the effectiveness of the photocatalyst. When the added dopant exceeds the optimum amount, an adverse effect is produced on the photocatalytic activity. This condition causes the band gap to become very small, leading to more accessible electron and hole recombination. Excessive dopant also initiates structural defects that serve as recombination centers [21]. Therefore, it is necessary to carry out further studies regarding the effect of Fe concentration on photocatalysts in photoelectrocatalytic combination systems to observe the synergistic effect between the electron and hole recombination process and the photocatalyst activity in visible light (band gap narrowing). It aims to increase glycerol degradation (waste elimination) and H_2 production simultaneously.

In this study, the effects of relevant parameters on the rate of H_2 production were investigated, including the initial concentration of glycerol and the amount of Fe loading (based on SILAR cycles) by utilizing the photoelectrocatalysis method as a combination of photocatalysis and electrolysis processes. Based on the information in the previous paragraphs, we claim that the effect of initial glycerol concentration and the amount of Fe loading on hydrogen production by photoelectrocatalysis is the academic novelty of this study. The photocatalyst samples were characterized using UV-Vis DRS, XRD, and FESEM/TEM/HRTEM. These results are expected to obtain effective, low cost, environmentally friendly and optimum operating conditions in a combined photoelectrocatalytic system of glycerol degradation and H_2 production under visible light radiation.

2. Materials and Methods

2.1. Photocatalyst synthesis and characterization

The materials used included titanium (Ti) plate (0.3 mm thick, 99.6% purity from Shaanxi Yunzhong Metal Technology Co., LTD), platinum (Pt) plate, distilled water, HF (Merck), HNO_3 (65%, Merck), glycerol, NH4F (Merck, 98%), $Fe(NO_3)_3.9H_2O$ (Merck, analytical grade), Na_2SO_4, and argon. Meanwhile, the equipment used included a stopwatch, magnetic stirrer, furnace, DC power supply, mercury, thermometer, pH meter, Nafion NR 117 membrane, sandpaper, Shimadzu C-R6A Chromatopac, and photoelectrocatalytic reactor equipped with mercury lamp.

The synthesis of Fe-TiO_2 nanotubes was carried out by electrochemical anodization method, which comprised three steps: preparation of Ti plate, anodization process, and SILAR method for the deposition of Fe dopant on TiO_2 nanotube (TiTNAs). Before anodizing, the Ti plate with 4 x 3 cm dimensions was sanded to remove any undesired particles and rinsed with distilled water. Subsequently, chemical polishing was conducted on the Ti plate using an acid solution of HF: HNO_3: H_2O with a volume ratio 1:3:46 for 2 minutes. The Ti plate was then sonicated for 10 minutes in distilled water to remove residual acid from the surface. Once cleaned, it was dried and stored in a desiccator to avoid oxide formation.

The anodization of Ti was carried out using 150 ml organic electrolyte solution containing glycerol, 0.5 %wt NH_4F, and 25 %(v/v) distilled water. This process employed a power supply of 50 V for 2 hours. Furthermore, the electrodes used were a Ti plate as an anode and a Pt plate as a cathode. After the anodization, the TiO_2 nanotubes were rinsed with distilled water and dried at room temperature. The Fe dopant, subsequently, was added using the SILAR (Successive Ionic Layer Adsorption and Reaction) method. The anodized

TiNTAs were immersed for 10 minutes under stirring using a magnetic stirrer in a $Fe(NO_3)_3.9H_2O$ precursor solution with a fixed concentration and different cycles for variations in the resulting Fe dopant loading. Afterwards, they were rinsed with distilled water for 30 seconds and dried at room temperature for 30 seconds. TiNTAs immersion until the drying process was counted as one SILAR cycle. The SILAR process was performed with a precursor concentration of 0.12 M, and variations in Fe dopant loading were conducted by changing the SILAR cycles into 5, 10, and 15. The doped TiNTAs were then calcined at 500°C for 3 hours to obtain a stable anatase crystal structure with a high fraction.

The characterization test was conducted to determine the physical and chemical properties of the synthesized photocatalyst. The band-gap energy was calculated using the UV-Visible Diffuse Reflection Spectra/DRS (Harrick Scientific, Agilent Cary 600 UV-Vis DRS). X-ray diffraction/ XRD analysis was carried out at an angle range of $2\theta = 10^o – 90^o$ with the beam source of the X-ray radiation was Cu Kα (λ = 0.15406 nm) at a voltage of 40 kV and a current of 30 mA. The Scherrer equation was employed to estimate the crystallite size of the photocatalyst using the full-width half maximum (FWHM) of XRD patterns data. Meanwhile, the morphology, structure and elemental composition were investigated using Field Emission Scanning Electron Microscope (FESEM, FEI Inspect F50, and JEOL JIB-4610F) and Transmission Electron Microscope (TEM, FEI Tecnai G2 20 S-Twin).

2.2. Photoelectrocatalysis experiment system

The photoelectrocatalytic test was performed to determine the effect of the SILAR cycle of Fe dopant and initial glycerol concentration for the resulting hydrogen production. In this test, glycerol degradation and hydrogen production occurred simultaneously. The modified TiNTAs nanotube was used as a photoanode, and the platinized Ti plate was as a cathode. A series of photoelectrocatalytic reactors for glycerol degradation is depicted below.

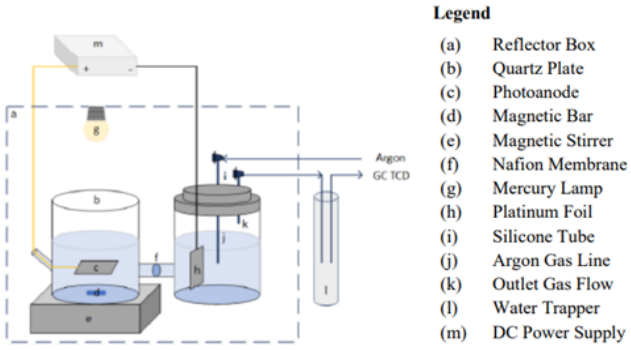

Fig. 1. Photoelectrocatalytic reactors for glycerol degradation

In the two PEC compartments, electrons flowed from the anode to the cathode under a DC power supply. Also, 200 ml of 10% glycerol was put in the photoanode cell compartment. TiO_2 nanotubes doped with Fe in up to 15 SILAR cycles were used as the anode in the photoanode cell compartment closed with a quartz plate. In total, 300 ml of 0.5 M Na_2SO_4 were added into the cathode cell compartment, and a platinized Ti plate was installed as a cathode. The anode and cathode were connected to the DC power supply. The electric potential was set constant at 1 Volt since at higher voltages there was no significant increase in the photocatalytic performance [22]. Before the reaction, a leak test and purging process were carried out by flowing low-pressure argon gas for 30 minutes. The mercury lamp (17.25% UV and 82.75% visible light, 250 W) and DC power supply were turned on and left for 120 minutes. Hydrogen production data were collected every 30 minutes, and the H_2 concentration was measured using gas chromatography (Shimadzu GC-8A equipped with a Molecular Sieve/MS Hydrogen 5 A column) at a certain retention time. This GC was directly connected to the reactor with argon as the carrier gas. The test was repeated at the initial concentrations of 0%, 2.5%, 5%, 7.5%, and 10% glycerol. Furthermore, this process was also repeated on various Fe dopant concentrations at SILAR cycles of 0, 5, 10, and 15.

3. Results and Discussion

The photocatalyst samples were named with codes as presented in Table 1.

Table 1. The naming of the photocatalysts refers to the variation of the experiments performed

Sample Code	Description
TiNTAs	TiO_2 Nanotube Arrays without dopant modification
TiNTAs ·5C	TiO_2 Nanotube Arrays with 5 SILAR cycles of Fe dopant modification
TiNTAs ·10C	TiO_2 Nanotube Arrays with 10 SILAR cycles of Fe dopant modification
TiNTAs ·15C	TiO_2 Nanotube Arrays with 15 SILAR cycles of Fe dopant modification

3.1. UV-Vis DRS Characterization of TiNTAs

The determination of photocatalysts' band gap and shift of light absorption by Fe-TiO_2 nanotubes was performed by UV-Vis DRS within a 300-800 nm wavelength range. Characterization with UV-Vis Diffuse Reflectance Spectroscopy (DRS) was based on the measurement of the UV-Vis light intensity reflected by the photocatalyst samples. When the ultraviolet or visible light was irradiated to the photocatalyst samples, some of it was transmitted, absorbed and reflected in the form of spectra. The light absorption caused the excitation of electrons from the ground to an excited state [23]. Figure 2 shows the y-axis as the photocatalyst absorbance of light with a wavelength of 250-500 nm on the x-axis. From that figure, it can be seen that the adding Fe dopant increased the photocatalyst absorbance ability in the visible light spectrum. The increase in the absorbance of Fe-doped TiNTAs in visible light was due to the presence of ionic impurities Fe^{3+} formed within the TiO_2 matrix, causing changes in TiO_2 band structure.

Using the Kubelka-Munk function and Tauc plot, the value of the band gap energy of each sample could be observed. The band-gap value was determined by plotting $(F(R)hv)^{0.5}$ curve against energy, hv (eV), called as Tauc plot with $F(R) = (1-R)^2/2R$, R = reflectance, and hv = photon energy. The band gap energy could be found by extrapolating the linear region of the Tauc plot until it intersected the x-axis [14]. Based on the

analysis, Fe-TiNTAs had a lower energy band gap than their standard counterpart (Figure 2 inset). The band-gap energy of Fe-TiNTAs with 5, 10, and 15 SILAR cycles of $Fe(NO_3)_3$ as Fe precursor were 3.08 eV, 2.9 eV, and 2.74 eV respectively, which were smaller compared to the pure photocatalyst (3.15 eV). The decreasing band-gap energy was due to Fe dopant presence in the photocatalyst. $Fe(NO_3)_3$ had less band-gap energy than pure TiNTAs; therefore, absorption was extended to the visible light region.

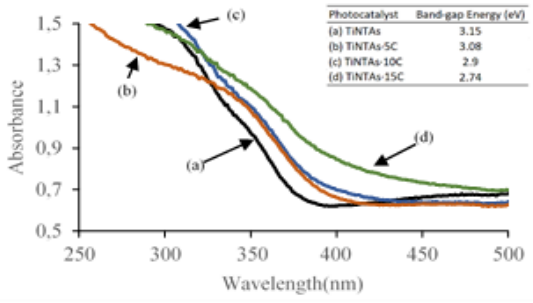

Fig. 2. UV-Vis DRS absorbance spectra of various photocatalysts

3.2. XRD characterization of TiNTAs

XRD (X-Ray Diffraction) characterization was conducted to observe the crystalline phase and crystalline size of TiNTAs and Fe-TiNTAs, and the results are presented in Figure 3. The TiNTAs-15C was a sample with Fe dopant addition using the SILAR method for 15 cycles. There are six diffraction patterns of anatase crystals at 2θ = 25.36°, 37.9°, 48.09°, 54°, 55.12°, and 62.78° corresponding to the diffraction peaks of the anatase phase in the planes (101), (104), (200), (105), (211), and (204) respectively (JCPDS No. 21-1272). Another diffraction peak, namely titanium, was observed at 2θ = 35.16°, 38.44°, 40.23°, 53.05°, and 63.04° (JCPDS No. 21-1272) [24]. As seen by position, there was almost no difference between TiNTAs and TiNTAs-15C composites. However, there were some differences in the height of the anatase and titanium peaks in both photocatalysts, which affected the crystal size. These may arise due to the thermal treatment or calcination process with high temperatures in the production of TiNTAs-15C composites, which caused an increase in the crystal size of the anatase catalyst. Increasing the crystalline size may also be caused by the higher conductivity of Fe (79.5 W/mK) compared to the pure TiO_2 (4.8 W/mK). Higher conductivity promotes better heat conductivity and facilitates the formation of anatase crystals during the calcination process [25]. No diffraction was observed in the XRD patterns for iron-based oxides. The absence of a new diffraction peak for the TiNTAs-15C may be due to the characterization technique used, which was not very sensitive to the low concentration of Fe^{3+} and may also be due to the Fe^{3+} substituting Ti^{4+} in the TiNTAs lattice structure. Another reason was that Fe in the form of Fe^{3+} stuck to the surface of amorphous TiO_2, a type of solid with an irregular non-crystalline structure that XRD does not detect.

The absence of rutile peaks at 2θ = 27.4° and 36° in the XRD results of TiNTAs and TiNTAs-15C indicated that the synthesized photocatalysts were 100% anatase phase because calcination occurred at 500°C. Anatase crystals on the TiO_2 photocatalyst are the most active in photocatalysis due to their larger surface area and more active sites. The higher the number of anatase crystals in the photocatalyst, the better the effectiveness of the photocatalytic performance. However, the presence of rutile crystals also means that the photocatalyst is no longer amorphous and more crystalline without impurities. A catalyst containing both anatase and rutile should have greater anatase than the rutile to ensure optimum effectiveness in photocatalysis.

From FWHM data, the crystal size of the synthesized photocatalyst was calculated using the Scherrer equation L = K.λ/ βcosθ [4,26] where L is the crystallite size, K is the Scherrer constant (0.9), λ is the wavelength of the X-rays radiation used (0.15406 nm), β is the Full Width at Half Maximum (FWHM, radians), and θ is the peak position (radians). The result is presented in Figure 3 inset. To determine the value of FWHM (β) has been explained clearly by other researchers [26]. The presence of Fe TiNTAs-15C increased the crystallite size from 26 to 29 nm for the TiNTAs and Fe-TiNTAs respectively (Figure 3 insert).

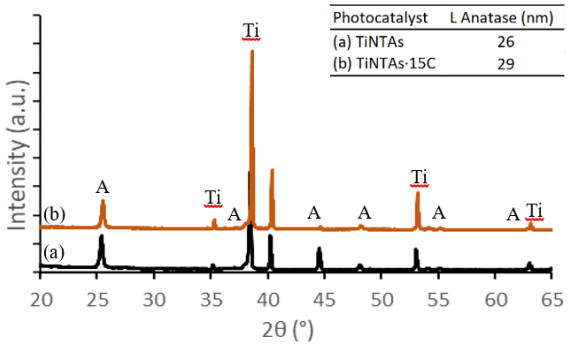

Fig. 3. XRD Spectra of (a) TiNTAs and (b) TiNTAs-15C

3.3. FESEM-EDX characterization of TiNTAs

The characterization of FESEM (Field Emission Scanning Electron Microscopy) aimed to determine the morphology and structure of TiNTAs, while EDX aimed to identify the type of atom attached to the surface. This characterization employed Thermo Scientific – Quattro S with high vacuum mode, 15 kV, and 4.0 spot size. Figure 4 shows the FESEM results, comparing the nanocomposite morphology at 20,000 times magnification on pure TiNTAs and on Fe-TiNTAs. As seen from the figure, the addition of Fe on TiNTAs was insignificantly different from the nanotubular structure and morphology of TiNTAs, most likely due to the small amount of Fe deposited. Fe deposited into TiNTAs up to 15 SILAR cycles caused no agglomeration.

The procedures for interpreting and calculating the average tube inner diameter and tube wall of TiNTA have been explained in previous paper [27,28]. The average tube inner diameter of all photocatalyst samples ranged between 221 and 303 nm; meanwhile, the average tube wall thickness was between 27 and 37 nm (Table 2). It is reported that the mixing process and water content during anodization may affect the final size and nanotubular structure of TiNTAs [27]. This phenomenon occurs because there is a competition between the dissolution of TiO_2 into the electrolyte solution at the top of the tube and the formation of TiO_2 in the bottom tube during anodization.

Table 2 shows that increasing the Fe dopant loading through the SILAR cycle decreased the average tube diameter. In

contrast, there was no significant effect on the tube wall thickness. The tube diameter decreased because Fe^{3+} possessed a great electron affinity, which could easily enter the Ti^{4+} crystal lattice. As a result, the attractive force with O atoms became stronger, leading to the nanotube shrinkage. The decrease in the tube diameter was accompanied by an increase in the number of tubes formed.

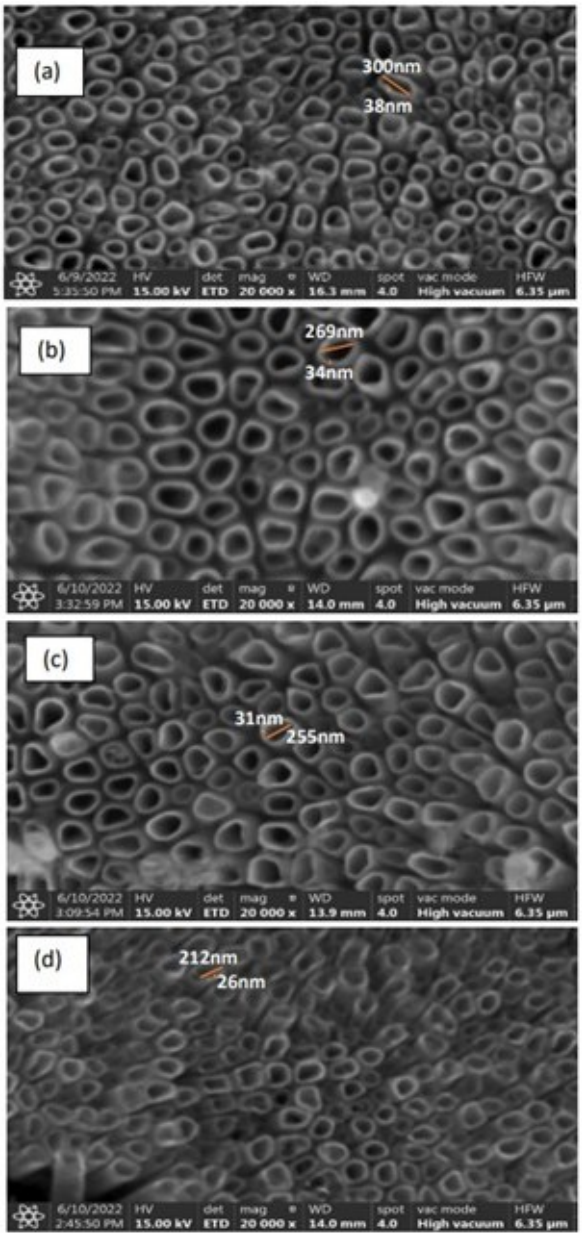

Fig. 4. FESEM of deferent Photocatalysts (a) TiNTAs, (b) TiNTAs·5C, (c) TiNTAs·10C, (d) TiNTAs·15C

Based on the EDX results, the increase in the SILAR cycle on TiNTAs was positively correlated with the %w of Fe, although not proportional. The mass percentage of the Fe component on the photocatalysts according to the number of cycles 0, 5, 10, and 15 was 0%, 0.2%, 0.6%, and 0.6%, respectively. It means that Fe nanoparticles had been successfully doped on the TiNTAs photocatalyst. The non-linear relationship between the SILAR cycle and Fe deposited on TiNTAs was caused by TiNTAs having limited active sites for attaching Fe particles. Therefore, linearity only occurred at low Fe precursor concentrations. Furthermore, Fe reached saturation on the TiO_2 surface at a high Fe concentration.

Table 2. TiNTAs dimension and elemental composition

Photo-catalyst	Avg. Diameter (nm)	Avg.Wall Thickness (nm)	wt% Fe (from EDX analysis)
TiNTAs	303	33	0
TiNTAs ·5C	271	37	0.2
TiNTAs ·10C	254	31	0.6
TiNTAs ·15C	221	27	0.6

Figure 5 presents the TEM and HRTEM imaging that further proved the deposition of Fe distributed on the TiNTAs surface. Figure 5(a) shows the image of the middle nanotube, and it confirmed that Fe was well dispersed on the tube wall and the tube mouth of TiNTAs with the tube diameter of ca 221 nm and the wall thickness of ca 27 nm. This further corroborated our FESEM results as presented in Table 2. According to Figure 5(b), the d-spacing value of 0.359 nm corresponded to the presence of the anatase crystal phase (101) of TiO_2. On the other hand, lattice fringes of 0.687 nm confirmed the presence of Fe_2O_3 with the crystal phase (002). This finding is in good agreement with the previous study [29].

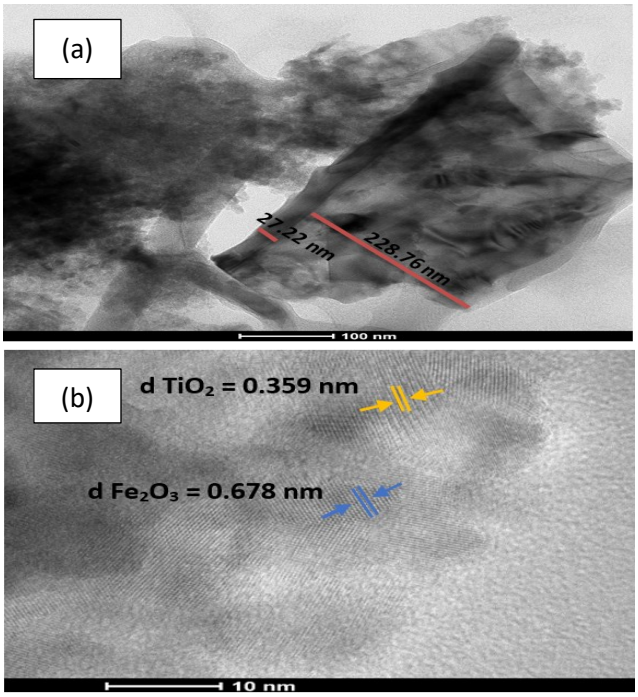

Fig. 5. (a) TEM and (b) HRTEM of TiNTAs·15C

3.4. Variations of photocatalysis, electrolysis, and photoelectrocatalysis methods in H_2 production

Photocatalysis is a process that uses light on a catalyst to accelerate its chemical transformation. An electrolysis process can be added to the photocatalysis to eliminate the high recombination rate of photo-generated electron-hole pairs. This combination is then called as photoelectrocatalysis. This addition is believed to increase the quantum efficiency of TiNTAs due to its capability to promote the electrons generated on the anode side to be transferred to the cathode by an external circuit to suppress charge recombination. Figure 6 shows the

accumulation of hydrogen production from each photocatalysis, electrolysis, and photoelectrocatalysis process for 2 hours. There is a significant improvement of photoelectrocatalytic processes compared to the individual process as depicted in Figure 6. In 2 hours, photocatalysis, electrolysis, and their combination produced hydrogen of 78.06, 104.39, and 404.39 mmol/m^2, respectively. The photoelectrocatalytic process could generate H_2 about 4-5 times greater than the single process. This phenomenon proves that the photocatalytic process can synergize with the electrolysis to produce hydrogen.

The photocatalytic activity is enhanced in the photoelectrocatalytic system due to the applied external bias. In the external bias application, the photoexcited electrons in the valence band are directly transferred to the cathode, thereby suppressing electron-hole recombination. This condition causes the holes to focus on glycerol oxidation, which can increase the production of hydrogen ions. Subsequently, more hydrogen ions generated are transferred to the cathode cell compartment through the Nafion membrane. Additionally, more electrons are transferred to the cathode, where hydrogen ions from glycerol oxidation are reduced to H_2 [30]. The mechanism that may occur in glycerol photodegradation by TiO_2 in the photoelectrocatalytic process is presented as follows [31]:

- Anode reactions

$$TiO_2 + hv \rightarrow TiO_2\ (h^+ + e^-) \quad (1)$$

$$C_3H_8O_3 + 3H_2O + 14h^+ \rightarrow 3CO_2 + 14H^+ \quad (2)$$

- Cathode reactions

$$Pt + e^- \rightarrow Pt(e^-) \quad (3)$$

$$14H^+ + 14Pt(e^-) \rightarrow 7H_2 + 14Pt \quad (4)$$

- Overall reactions

$$C_3H_8O_3 + 3H_2O \rightarrow 3CO_2 + 7H_2 \quad (5)$$

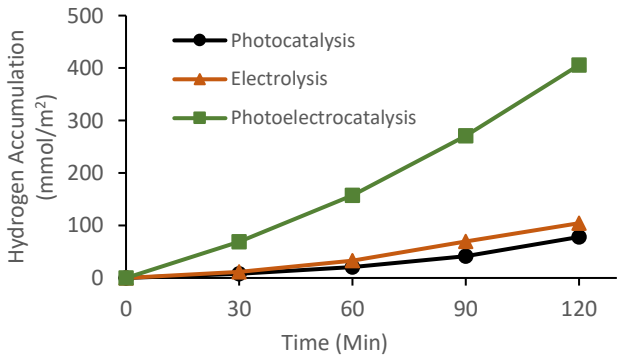

Fig. 6. H_2 production profile on various methods

3.5. Photoelectrocatalysis with varying number of Fe SILAR Cycle

In this study, TiNTAs were calcined under an oxidative atmosphere (air), and the calcined TiNTAs showed a better photocatalytic activity. However, Fe dopant was added to the TiNTAs before calcination using the SILAR method. This addition aimed to reduce the band gap energy and electron-hole recombination rate. During the experiment, the number of SILAR cycles varied, namely 0, 5, 10, and 15, to obtain the amount of Fe dopants attached to the catalyst surface to study their effect on the hydrogen produced.

Figure 7 shows the effect of variations in the number of SILAR cycles on the hydrogen produced in the photoelectrocatalysis process. The higher the number of SILAR cycles, the more hydrogen produced. Within two hours, the accumulation of hydrogen generated during photoelectrocatalysis at variation of 0, 5, 10, and 15 cycles was 164.89, 237.03, 317.97, and 405.8 mmol/m^2, respectively. The more cycles in the SILAR method, the more Fe deposited in TiNTAs, resulting in more H_2 being produced. This finding is in accordance with the EDX results (w% Fe), as seen in Table 2. Using TNTAs-15C photocatalyst could increase the H_2 produced during photoelectrocatalysis by ±2.5 times more than the un-doped photocatalyst. This condition proved that the more Fe deposited on the catalyst, the better the photoelectrocatalytic performance. The Fe dopant reduced the band gap energy (Figure 2 inset) and the electron-hole recombination rate. Reducing band gap energy could enhance light absorption in the visible region since the absorbance spectra of photocatalyst samples shifted to the visible light domain.

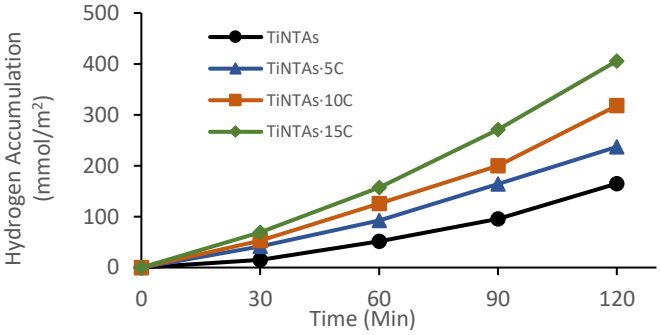

Fig. 7. H_2 production profile at various number Fe SILAR Cycles

3.6. Photoelectrocatalysis for variations of initial glycerol concentration

As stated previously, the photocatalytic process combined with electrolysis can suppress the electron-hole recombination. On the other hand, adding a sacrificial agent such as glycerol in photoelectrocatalysis can reduce the recombination rate. Based on the research conducted by Daskalaki, 2009 [32], the presence of glycerol as a reagent increased hydrogen production. It accelerated the reaction rate up to 1 order compared to the usual water-splitting reaction. The glycerol reaction that produces hydrogen is due to the presence of an alcohol group, which is easily oxidized. However, the glycerol waste found in the environment has varying concentrations. In this experiment, the initial waste concentration of glycerol was varied at 0%, 2.5%, 5%, 7.5%, and 10% to obtain the optimal concentration and analyze its effect on the hydrogen produced.

Figure 8 shows the effect of variations in the initial concentration of glycerol waste on the hydrogen produced in the photoelectrocatalysis process. The higher the glycerol concentration, the more hydrogen produced. Furthermore, in 2 hours, the accumulation of hydrogen produced at the initial concentration varied by 0%, 2.5%, 5%, 7.5%, and 10% was 65.6, 137.24, 232.99, 323.68, and 404.39 mmol/m^2,

respectively. The performance of photoelectrocatalysis at 10% glycerol concentration variation could increase the amount of hydrogen produced during the process by up to ± 6 times more once compared to 0%. This result showed that glycerol usage as a raw material for hydrogen production and a hole scavenger has successfully increased the H_2 generated.

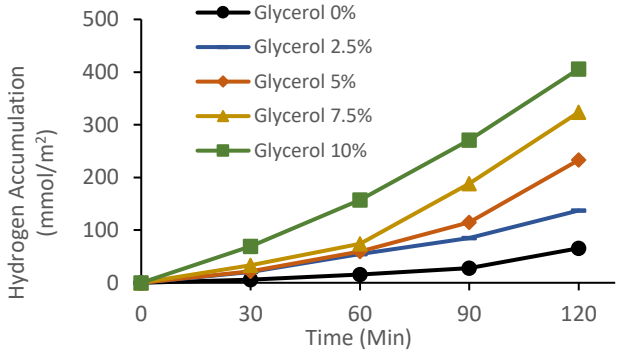

Fig. 8. H_2 production with various initial concentrations of glycerol

3.7. Photoelectrocatalysis for reuse of glycerol solution

Besides aiming to produce hydrogen, applying photoelectrocatalysis in glycerol solution could degrade the waste. Once TiO_2 was exposed to light (hv) with the appropriate energy, electrons (e^-) in the valence band (VB) were excited to the conduction band (CB), thereby forming a hole (h^+) in the VB left behind. The electrons and holes formed diffuse on the surface to form superoxide (O_2-) and hydroxyl radicals (·OH). These two radical species could oxidize organic species by producing CO_2 and H_2O [9].

The photoelectrocatalyzed solution was reused in this research to observe the hydrogen produced in each scheme. The H_2 generated in the first use was then compared to the second use of glycerol solution to determine the degradation rate during the process, as depicted in Figure 9. The results of hydrogen accumulation in the first and second use of glycerol solutions were 397.27 mmol/m^2 and 320.84 mmol/m^2, respectively as shown in Table 3. These results showed that the reuse of glycerol solution reduced hydrogen production due to glycerol degradation during the process. The estimated initial concentrations of glycerol waste in glycerol solutions' first and second use were 10% and 8.19%, respectively. This result proved that combining photoelectrocatalytic processes could play a role in simultaneous hydrogen production and glycerol waste degradation.

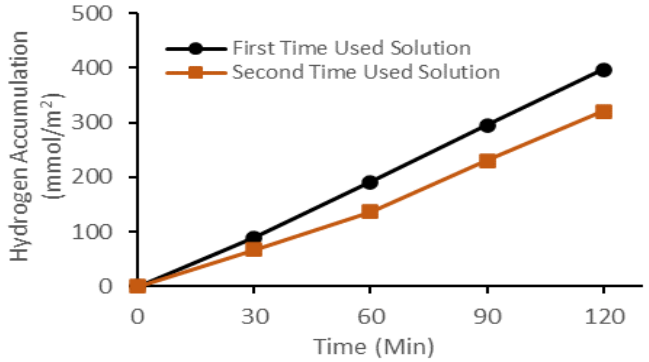

Fig. 9. H_2 production with variations of reused solution

Table 3. Glycerol Concentration Degradation

Photoelectrocatalytic Test	Total H2 Accumulation (mmol/m2)	Estimated Glycerol Concentration (%)
First-time usage	397.27	10%
Second-time usage	320.84	8.19%

4. Conclusion

Fe deposited on TiNTAs (Fe-TiNTAs) by the SILAR method has been successfully synthesized and proven by FESEM/EDX and HRTEM characterizations. The number of SILAR cycles affected the w% Fe deposited on TiNTAs, and this dopant was used as an electron/hole trapper, which could reduce the electron-holes recombination rate and narrow the band gap. Fe loading on TiNTAs, initial glycerol concentration and process combination (photoelectrocatalysis) in converting glycerol solution determined the H_2 produced. Meanwhile, increasing glycerol concentration as a raw material for hydrogen production and a hole scavenger has successfully elevated the amount of H_2 generated.

Acknowledgements

The authors are grateful for the financial support provided by the Ministry of Education, Culture, Research, and Technology of Indonesia (Kemendikbudristek RI) through the Decentralized "Penelitian Dasar Unggulan Perguruan Tinggi" Grant with contract number: NKB-997/UN2.RST /HKP.05.00/2022.

References

1. Y. Jie, et al., *WO_3-based materials for photoeletcrocatalytic glycerol upgrading into glyceraldehyde: Unravelling the synergistic photo-and electro-catalytic effects*, Appl. Catal. B Environ. 318 (2022) 121843.
2. H. L. Wei, V. Truong-Giang and C. Chia-Ying, *Converting glycerol aqueous solution to hydrogen energy and dihydroxxyacetone by the $BiVO_4$ photoelectrochemical cell*, Electrochim. Acta 322 (2019) 134725.
3. P. Mardina, H. Wijayanti, A. Tuhuloula, E. Hijriyati and Sarifah. *Corncob residue as heterogenous acid catalys for green synthesis of biodiesel: A short review*, Commun. Sci. Tech. 6 (2021) 60-68.
4. Slamet, Ratnawati, J. Gunzlazuardi and E. L. Dewi, *Enhanced photocatalytic activity of Pt deposited on titania nanotube arrays for the hydrogen production with glycerol as a sacrificial agent,* Int. J. Hydrog. Energy 42 (2017) 24014-24025.
5. Ratnawati, Slmaet, V. Wongso, J. Gunzlazuardi and M. Ibadurrohman, *A Comparative Study of Pt Depositing Methods (Chemical Reduction vs Photo-Assisted Deposition) onto TiO_2 Nanoparticles for Hydrogen Photo-Production*, J. Eng. Technol. Sci. 54 (2022) 220612.
6. A. B. D. Nandiyanto, R. Zaen, and R. Oktiani, *Correlation between crystallite size and photocatalytic performance of micrometer-sized monoclinic WO_3 particles,* Arab. J. Chem. 13 (2020) 1283–1296.
7. A.B.D. Nandiyanto, R. Ragadhita, R. Oktiani, A. Sukmafitri, and M. Fiandin, *Crystallite Sizes On The Photocatalytic Performance Of Submicron WO_3 Particles*, J. Eng. Sci. Technol. 15 (3) (2020) 1506 – 1519.
8. O. Arutanti, et al., *Influences of Porous Structurization and Pt Addition on*

the Improvement of Photocatalytic Performance of WO_3 Particles, ACS Appl. Mater. Interfaces 7 (5) 3009-3017.

9. S. Sood, A. Umar, S.K. Mehta, and S.K. Kansal, *Highly effective Fe-doped TiO_2 nanoparticles photocatalysts for visible-light-driven photocatalytic degradation of toxic organic compounds*, J. Colloid Interface Sci.. 450 (2015) 213-223.
10. Y. Ohama, and D. eds. V. Gemert, *Application of titanium dioxide photocatalysis to construction materials: state-of-the-art report of the RILEM Technical Committee 194-TDP*, Springer Science & Business Media 5 (2011).
11. R. Singh and S. Dutta, *Integrated photocatalytic hydrogen production and pollutants or wastes treatment: prospects and challenges*, Sustainable Fuel Technologies Handbook, (2021) 541-549.
12. A. Galinska, and J. Walendziewski, *Photocatalytic water splitting over Pt− TiO_2 in the presence of sacrificial reagents*, Energy Fuels 19(3) (2005) 1143-1147.
13. F. Fatmawati, G. Shintavia, L. Qadariyah, and M. Mahfud, *Production of Hydrogen from glycerol with Heating Convention Method based of γ-Alumina,* J. Teknik ITS 3(2) (2014) 146-150.
14. Ratnawati, J. Gunlazuardi, E. L. Dewi and Slamet, *Effect of $NaBF_4$ addioton on the anodic synthesis of TiO_2 nanotube arrays photocatalyst for production of hydrogen from glycerol-water soluyion*, Int. J. Hydrog. Energy 29 (2014) 16927-16935.
15. R. Paritiwi, M. Ibadurrohman, E.L. Dewi and Slamet, *A novel approach in the synthesis of CdS/titania nanotubes array nanocomposites to obtain better photocatlayst performance*, Commun. Sci. Technol. 8 (2023) 16-24.
16. J. S. Sagar, G. M. Madhu, J. Koteswararao and P. Dixit*, Studies on thermal and mechanical behavior of nano TiO_2-epoxy polymer composite*, Commun. Sci. Technol. 7 (2022) 38-44.
17. F. Riyanti, Hasanudin, A. Rachmat, W. Purwaningrum, and P. L. Hariani, *Photolacatalytic degradation of methylene blue and Congo red dyes from aqueous solutions by bentonite-Fe_3O_4 magnetic*, Commun. Sci. Technol. 8 (2023) 1-9.
18. P. Roy, S. Berger and P. Schmuki, *TiO_2 nanotubes: synthesis and applications*, Angew. Chem. Int. Ed. 50 (2011) 2904-2939.
19. E. D. Rokhmawati, *Analysis of Dopant Selection in Reducing Band Gap Energy in TiO_2 Layer Synthesis,* In Seminar Nasional Lontar Physics Forum (2019) 42-46.
20. R. Dholam, N. Patel, M. Adami, and A. Miotello, *Hydrogen production by photocatalytic water-splitting using Cr-or Fe-doped TiO_2 composite thin films photocatalyst*, Int. J. Hydrog. Energy 34 (2009) 5337-5346.
21. A.E.R. Mohamed and S. Rohani*, Modified TiO_2 nanotube arrays (TNTAs): progressive strategies towards visible light responsive photoanode, a review*, Energy Environ. Sci. 4 (2011) 1065-1086.
22. T. Elysabeth, K. Mulia, M. Ibadurrohman, and E. L. Dewi, *A comparative study of CuO deposition methods on titania nanotube arrays for photoelectrocatalytic ammonia degradation and hydrogen production*, Int. J. Hydrog. Energy 46 (2021) 26873-26885.
23. R.A. Pratiwi, and A. B. D Nandiyanto, *How to Read and Interpret UV-VIS Spectrophotometric Results in Determining the Structure of Chemical Compounds*, Indones. J. Edu. Res. and Technol. 2(1) (2022) 1-20.
24. X. Shi, et al., *A mild in-situ method to construct Fe-doped cauliflower-like rutile TiO_2 photocatalysis for degredation of organic dye in wastewater*, Catal. 9 (2019) 426.
25. R. Muttaqin, et al., *Degradation of methylene blue-ciprofloxacin and hydrogen production simultaneously using combination of electrocoagulation and photocatalytic process with Fe-TiNTAs*, Int. J. Hydrog. Energy 47 (2022) 28272-18284.
26. S. Fatimah, R. Ragadhita, D.F. Al Husaeni, and A.B.D. Nandiyanto, *How to Calculate Crystallite Size from X-Ray Diffraction (XRD) using Scherrer Method*, ASEAN J. Sci. Eng. 2 (1) (2022) 65-76.
27. S. Slamet, L.F. Pelawi1, M. Ibadurrohman1, and R. Yudiant, Ratnawati, *Simultaneous Decolorization of Tartrazine and Production of H_2 in a Combined Electrocoagulation and Photocatalytic Processes using CuO-TiO_2 Nanotube Arrays: Literature Review and Experiment,* Indones. J. Sci. Technol. 7(3) (2022) 385-404.
28. Y.D. Yolanda, and A.B.D. Nandiyanto, *How to Read and Calculate Diameter Size from Electron Microscopy Images*, ASEAN J. Sci. Eng. Edu. 2(1) (2022) 11-36.
29. M. Ismael, *Enhanced photocatalytic hydrogen production and degredation of organic pollutants from Fe (III) doped TiO_2 nanoparticles*, J. Environ Chem. Eng. 8 (2020) 103679.
30. V. Kumaravel, S. Mathew, J. Bartlett, and S.C. Pillai, *Photocatalytic hydrogen production using metal-doped TiO_2: A review of recent advances*, Appl. Catal. B Environ. 244 (2019) 1021-1064.
31. I. Papagiannis, N. Balis, V. Dracopoulos and P. Lianos, *Photoelectrocatalytic Hydrogen Peroxide Production Using Nanoparticulate WO3 as Photocatalyst and Glycerol or Ethanol as Sacrificial Agents*, Processes 8 (2019) 37.
32. V. M. Daskalaki and D. I. Kondarides, *Efficient production of hydrogen by photo-induced reforming of glycerol at ambient conditions*, Catal. Today 144 (2009) 75-80.